

OPTICAL AND X-RAY CLUSTERS AS TRACERS OF THE SUPERCLUSTER-VOID NETWORK.
III DISTRIBUTION OF ABELL AND APM CLUSTERSMARET EINASTO¹, JAAN EINASTO¹, ERIK TAGO¹, HEINZ ANDERNACH², GAVIN B. DALTON³, AND
VOLKER MÜLLER⁴*Draft version November 10, 2018*

ABSTRACT

We present a comparison of Abell and Automated Plate Measuring Facility (APM) clusters of galaxies as tracers of the large scale structure of the Universe. We investigate selection functions of both cluster catalogs, using samples of all clusters (including clusters with estimated redshifts), and samples of clusters with measured redshifts. We find that the distribution of rich superclusters, defined by all Abell and APM clusters, is similar in volume covered by both cluster samples. We show that the supercluster-void network can be traced with both cluster samples; the network has a well-defined period of $\sim 120 h^{-1}$ Mpc. We calculate the correlation function for Abell and APM cluster samples. However, the APM cluster sample with measured redshifts covers a small volume which contains only a few very rich superclusters. These superclusters surround one void and have exceptionally large mutual separations. Due to this property the secondary maximum of the correlation function of APM clusters with measured velocities is located at larger scales than corresponding feature in the correlation function of Abell clusters. We conclude that the APM sample is not representative for the large-scale structure as a whole due to the small space coverage. The Abell cluster catalog is presently the best sample to investigate the large-scale distribution of high-density regions in the Universe. We present a catalog of superclusters of galaxies, based on APM clusters up to a redshift $z_{lim} = 0.13$.

Subject headings: cosmology: observations – large-scale structure of the Universe – cosmology: observations – cluster of galaxies

1. INTRODUCTION

In the present series of papers we study the properties of the supercluster-void network as delineated by different types of clusters of galaxies, as well as the regularity of this network. So far the supercluster-void network has been studied in detail only using samples of Abell clusters of galaxies (Abell 1958, Abell, Corwin, Olowin 1989, hereafter ACO). In the first two papers of this series we compared the distribution of Abell clusters with clusters selected on the basis of their X-ray emission (Einasto et al. 2001, Paper I) and derived their correlation functions (Tago et al. 2001, Paper II). Here we continue the comparison of samples of clusters of galaxies as tracers of the supercluster-void network, and now use the cluster catalog derived from scans with the Automated Plate Measuring (APM) Facility (Dalton et al. 1997, hereafter D97) based on the APM galaxy catalog (Maddox, Efstathiou & Sutherland 1996). One reason to compare the Abell and APM samples of clusters is the fact that power spectra derived from these cluster samples are different from each other. The power spectrum of Abell clusters has a sharp peak around the scale $l \approx 120 h^{-1}$ Mpc or wavenumber $k = 2\pi/l = 0.05 h \text{ Mpc}^{-1}$ (Einasto et al. 1997a, hereafter E97a, Retzlaff et al. 1998, hereafter R98). In contrast, the maximum of the power spectrum of APM clusters occurs on larger scales, $k \approx 0.04 h \text{ Mpc}^{-1}$, and it is flatter (Tadros et al. 1998, hereafter T98). The reason for these discrepancies is not fully clear. An independent study of Miller

& Batuski (2000) has shown only a mild feature on a scale $k = 0.05 h \text{ Mpc}^{-1}$, and the amplitude of the power spectrum increases toward larger scales.

The main goal of this paper is to compare the distribution of Abell and APM clusters of galaxies and to find how well these cluster catalogs can be used to investigate properties of the supercluster-void network. We shall use a cosmographic approach to describe superclusters and voids; we shall also apply various methods to quantify the distribution to allow the comparison of observations with theory.

The paper is organized as follows. In Section 2 we describe the cluster catalogs used: the latest compilation of redshifts of Abell clusters by Andernach & Tago (1998), and the published catalog of APM clusters by D97. We derive selection functions for both samples. In Section 3 we find the multiplicity function of superclusters in the APM catalogs, compile a supercluster catalog for the APM sample, and compare the distribution of rich superclusters in the Abell and APM catalogs; a supercluster catalog based on Abell sample was compiled in Paper I. To characterize the distribution of clusters in quantitative terms in Section 4 we derive the correlation function and power spectrum; we also investigate the distribution of neighbors of superclusters. We discuss our results and compare them with results of other studies in Section 5. Section 6 summarizes the main conclusions. In the Appendix we give a catalog of superclusters constructed on the basis of APM clusters, using a redshift limit $z_{lim} = 0.13$; it is also available electronically at the web site <http://www.aai.ee>.

¹Tartu Observatory, EE-61602 Tõrvavere, Estonia²Depto. de Astronomía, Univ. Guanajuato, Apdo. Postal 144, Guanajuato, C.P. 36000, GTO, Mexico³University of Oxford, Department of Astrophysics, Keble Road, Oxford, OX1 3RH, U.K.⁴Astrophysical Institute Potsdam, An der Sternwarte 16, D-14482 Potsdam, Germany

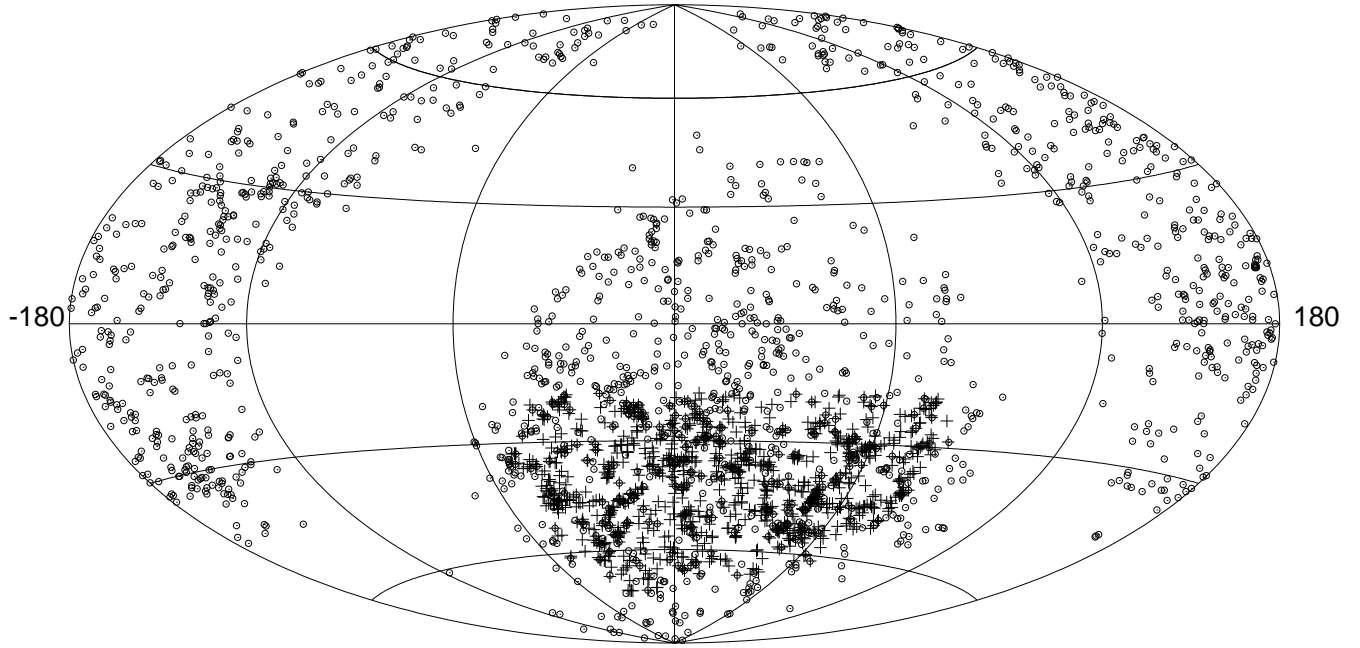


FIG. 1.— The distribution of Abell and APM clusters on the sky in equatorial Aitoff coordinates, plotted as open circles and crosses, respectively. Declination δ and right ascension are given in degrees, both for the equinox 1950. To avoid splitting of the region covered by APM sample, the zero point of the right ascension is put in the middle of the plot.

2. THE COMPARISON OF ABELL AND APM CLUSTER CATALOGS

2.1. Selection effects in Abell and APM cluster catalogs

For the present study we use the version of March 1999 of the redshift compilation for Abell clusters described by Andernach & Tago (1998). This compilation contains all known measured redshifts of Abell clusters, based on redshifts of individual cluster galaxies, and redshift estimates on the basis of the 10th brightest member of the cluster according to the formula derived by Peacock & West(1992), for both Abell catalogs (Abell 1958 and ACO). We omitted from the compilation all supplementary, or S-clusters, but included clusters of richness class 0. From this general sample we selected all clusters with measured redshifts not exceeding $z_{lim} = 0.15$. If no measured redshift was available we applied the same criterion for estimated redshifts. This sample contains 2276 clusters, 1258 of which have measured redshifts. We consider that a cluster has a measured redshift if at least one of its member galaxy has a measured redshift. In cases where the cluster has less than three galaxies with measured redshifts, and the measured and estimated redshifts differ by more than a factor of two ($|\log(z_{meas}/z_{est})| > 0.3$), the estimated redshift was used. In the case of component clusters (A,B,C etc) with comparable number of measured redshifts, we used only the cluster which better matches the estimated redshift.

The APM cluster catalog by D97 contains 957 clusters, 374 of which have measured redshifts. This cluster catalog was selected using the apparent magnitude limit, $m_X = 19.4$, as a distance indicator. This distance indicator is similar to Abell's magnitude m_{10} of the 10th brightest

galaxy in the cluster, used as distance indicator for the Abell catalog. In the case of the APM catalog the rank $X = C_i$ is calculated from the sum of weights of galaxies brighter than m_i ; i is the rank of the galaxy in the list ordered by magnitude; $C_i = X = 10$ is equivalent to Abell's rank m_{10} (for details see D97). The apparent magnitude limit $m_X = 19.4$ corresponds to a limit in the estimated redshift, $z_{est} = 0.118$.

The distribution of both ACO and APM clusters of galaxies on the sky is shown in Figure 1. We see that the APM cluster sample covers an area much smaller than the area covered by Abell clusters. We shall estimate the effective area and volume of both cluster samples in Section 5.2. The decrease of the surface density of Abell clusters towards the Galactic equator is well seen, and later in this Section we determine this dependence quantitatively. For the APM sample the surface density of clusters seems to be constant. However, as our analysis shows, here the surface density also depends on the Galactic latitude.

As a first step to investigate the selection effects in both cluster catalogs we looked for the relationship between estimated and measured redshifts (Figure 2). As noted above, the Abell cluster sample was selected using an upper limit of measured redshifts, $z_{lim} = 0.15$; if, instead, no measured redshift were available, a similar upper limit was applied for estimated redshifts. An inspection of Figure 2 shows that there exists a population of clusters with $z_{meas} < 0.15$ and $z_{est} > 0.15$. This is due to errors in estimated redshift. Thus it is natural to expect that some clusters within our distance limit have estimated redshifts above this limit. The preponderance of points *below* the line $z_{meas} = z_{est}$ is due to a preferred assignation of foreground galaxies to the

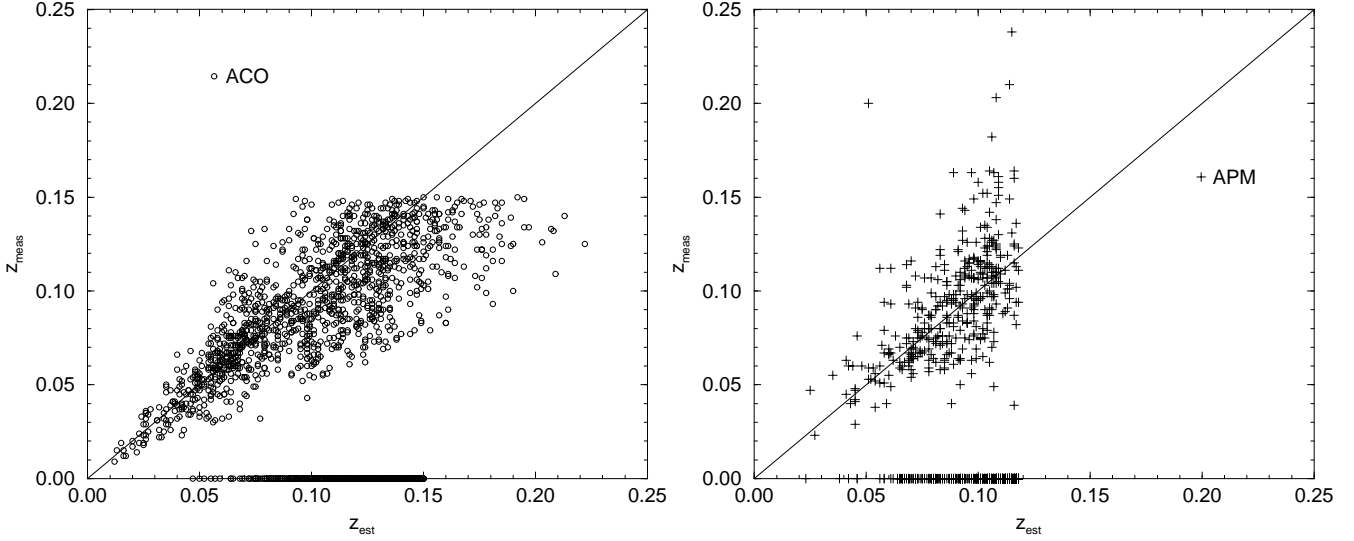


FIG. 2.— The relation between the measured and estimated redshift for Abell and APM cluster samples. The straight line is $z_{meas} = z_{est}$.

cluster as compared to background galaxies.

The APM cluster sample was constructed in a different manner. Here clusters were preselected for the redshift observing program using an *upper limit for the estimated redshift*, $z_{lim} = 0.118$. Since estimated redshifts are subject to random errors, some clusters of this sample have measured redshifts exceeding this limit. Similarly, some clusters that are located within the sphere of radius $z = 0.118$, are not included in the observing program since their estimated redshifts are larger than their true redshifts. This causes a large deficit of clusters near the far side of the sample, as we see below.

We convert the redshifts into radial distances r using the formula by Mattig (1958) as in Paper I. We adopt $H_0 = h 100 \text{ km s}^{-1} \text{ Mpc}^{-1}$, and $q_0 = \Omega_0/2 = 0.5$. Ω_0 is the density parameter (baryonic and dark matter) in units of the critical density.

In Figure 3 we plot the spatial density of clusters of galaxies in concentric shells of thickness $20 h^{-1} \text{ Mpc}$ in arbitrary units. Densities were calculated from the number of clusters in respective shells, divided by the volume of the shell (including regions not observed, thus this diagram cannot be directly used to calculate absolute spatial densities of clusters). To avoid a very small test volume in our vicinity, the first shell is taken between radii $r = 0$ and $r = 40 h^{-1} \text{ Mpc}$. We are interested in the spatial distribution of clusters in superclusters of different richness, which is defined as the number of clusters in superclusters, N_{cl} . Thus we plotted densities of clusters that belong to superclusters using a lower limit of supercluster richness, $N_{cl} \geq 1$ (all clusters of the sample, including isolated clusters), $N_{cl} \geq 4$, and $N_{cl} \geq 8$, i.e. clusters in superclusters with at least 4 or 8 members (E97d). Supercluster catalogs shall be discussed in the next subsection. They were constructed separately for all clusters, and for clusters having measured redshifts, both for the Abell and APM cluster samples.

Figure 3 shows that the spatial density of all clusters in the Abell catalog (sample ACO.A1, see Table 1 below) has a maximal spatial density near the observer. The density decreases slowly up to a distance $r \approx 375 h^{-1} \text{ Mpc}$; at this distance the spatial density is approximately 75 % of its lo-

cal value. At larger distances the density rapidly decreases to zero at the formal upper limit of the catalog that corresponds to a distance $r = 405 h^{-1} \text{ Mpc}$. It is interesting to note that the spatial density of clusters located in rich ($N_{cl} \geq 4$) and very rich ($N_{cl} \geq 8$) superclusters follows the same trend, though at lower density levels, except at very small distances where the density of clusters in very rich superclusters drops to zero due to the absence of nearby very rich superclusters. We see also that on distances up to $r \approx 200 h^{-1} \text{ Mpc}$ almost all clusters have measured redshifts; the fraction of measured redshifts slowly decreases to about 50 % at $r = 300 h^{-1} \text{ Mpc}$, and to about 30 % at $r = 350 h^{-1} \text{ Mpc}$.

The spatial density of APM clusters shows a completely different dependence on distance. There are no APM clusters at small distances, $r \leq 50 h^{-1} \text{ Mpc}$, and almost no clusters in rich and very rich superclusters at distances less than $150 h^{-1} \text{ Mpc}$. The overall density of the sample increases approximately linearly with increasing distance up to $r = r_{max}$, and thereafter drops suddenly to zero at $r = 350 h^{-1} \text{ Mpc}$ for clusters in superclusters; there is a very sparse extension of the distribution of isolated clusters up to a distance $r \approx 450 h^{-1} \text{ Mpc}$. At small distances almost all clusters have measured redshifts; with increasing distance the fraction of clusters with measured redshifts continuously decreases; near the maximum of the spatial density only 1 of 6 clusters has a measured redshift.

The selection function in Galactic latitude, b , is plotted in Figure 4 where surface density of clusters is expressed in arbitrary units. As argument we use $\sin b$, which is proportional to surface area. We do not distinguish between northern and southern Galactic hemispheres of the Abell sample and plot a merged distribution. Figure 4 shows that the surface density decreases almost linearly with the decrease of $\sin b$. This effect was noticed already by Einasto et al. (1997b, hereafter E97b), and by E97d. Conventionally the selection effect in Galactic latitude is taken into account by cutting the sample at some latitude ($|b| \approx 30^\circ$), and ignoring the latitude dependence at high latitudes. As we see, the latitude dependence exists also at high latitudes, and cannot be ignored. Figure 4 also shows that the difference

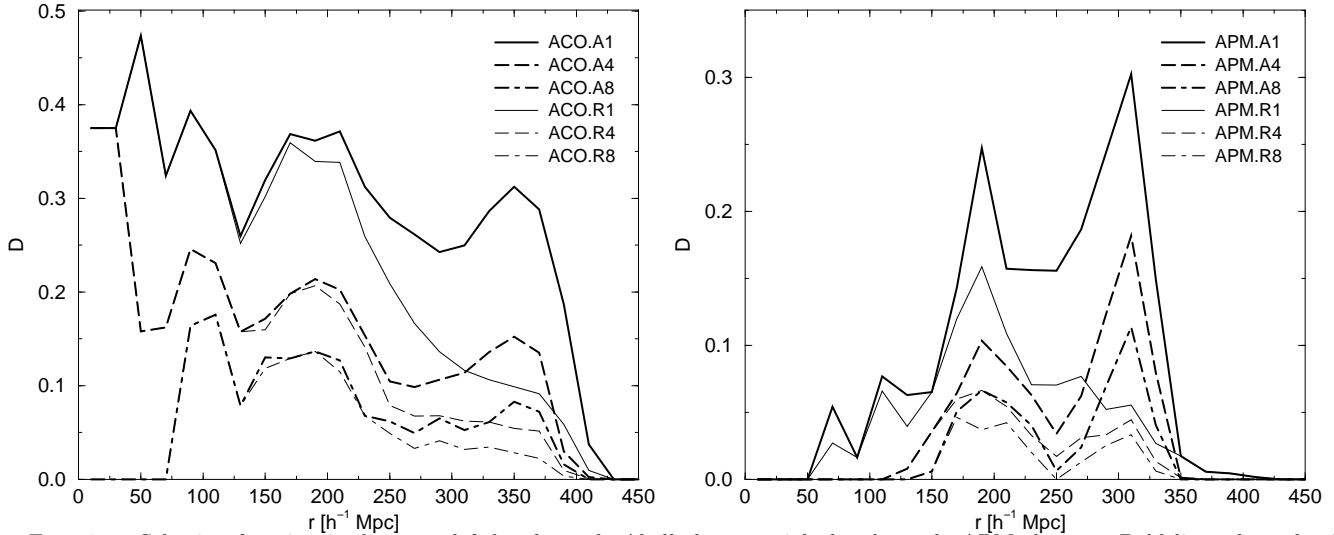


FIG. 3.— Selection function in distance; left-hand panel: Abell clusters; right-hand panel: APM clusters. Bold lines show the distribution of all clusters, thin lines the distribution of clusters with measured redshifts. Solid lines are for clusters in superclusters of all richness classes (including isolated clusters), dashed and dot-dashed lines are for clusters, located in superclusters of multiplicity $N_{cl} \geq 4$ and $N_{cl} \geq 8$, respectively.

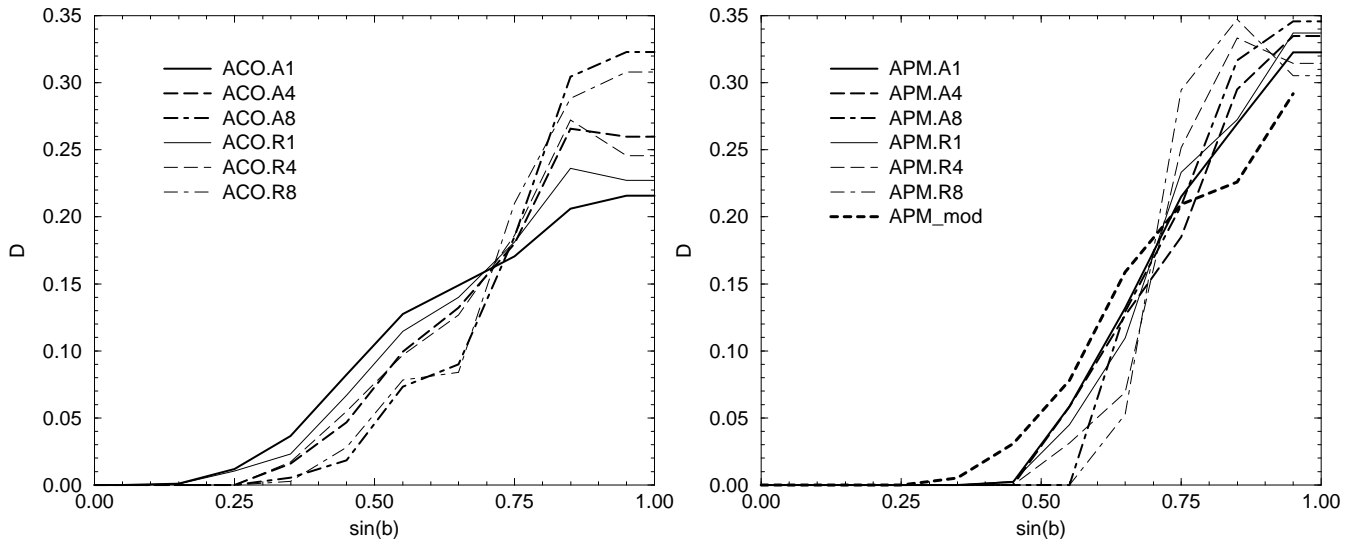


FIG. 4.— Selection function in Galactic latitude. Left hand panel: Abell clusters; right hand panel: APM clusters. Designations are as in Figure 3. The bold short-dashed line in the right panel shows the selection function for a model that covers the region observed by APM cluster survey with homogeneous surface density of test points.

between the latitude selection of all clusters and clusters with measured redshifts is small. A much steeper dependence exists for clusters in rich and very rich superclusters. We shall discuss this difference in more detail in Section 5.

The latitude dependence for APM clusters is shown in the right panel of Figure 4. The APM sample covers a restricted area around the southern Galactic pole, thus the latitude dependence is steeper than in the case of Abell clusters. For comparison we plot the latitude dependence for a model; it consists of 4000 points evenly distributed on the sky between $-50^\circ \leq RA \leq 80^\circ$ and $-0.95 \leq \sin \delta \leq -0.30$, covered by the APM sample. Figure 4 shows that the actual distribution of APM clusters has a steeper latitude dependence than the model; in other words, the APM sample is subject to latitude selection effects similar to that for the Abell sample. We shall discuss selection effects in more detail in section 5.1.

Our previous studies of the correlation function and power spectrum show that on large scales these functions are determined by clusters located in high-density regions, i.e. in rich and very rich superclusters (E97b, Einasto et al. 1997c, hereafter E97c). Sparse samples, where superclusters cannot be determined, have little or no influence on these functions. For this reason we shall use for further study only cluster samples in a volume within a limiting radius $r_{lim} = 350 h^{-1} \text{ Mpc}$, which corresponds to a limiting redshift of approximately $z_{lim} = 0.13$. Beyond this distance the spatial density of Abell clusters decreases rapidly. We apply this distance limit to Abell and APM samples. Data on samples used for further study are given in Table 1. These samples are designated as follows: the first 3 letters, ACO or APM, denote clusters from the respective catalogs; the following capital letter denotes samples of all clusters, (“A” including clusters with estimated redshifts),

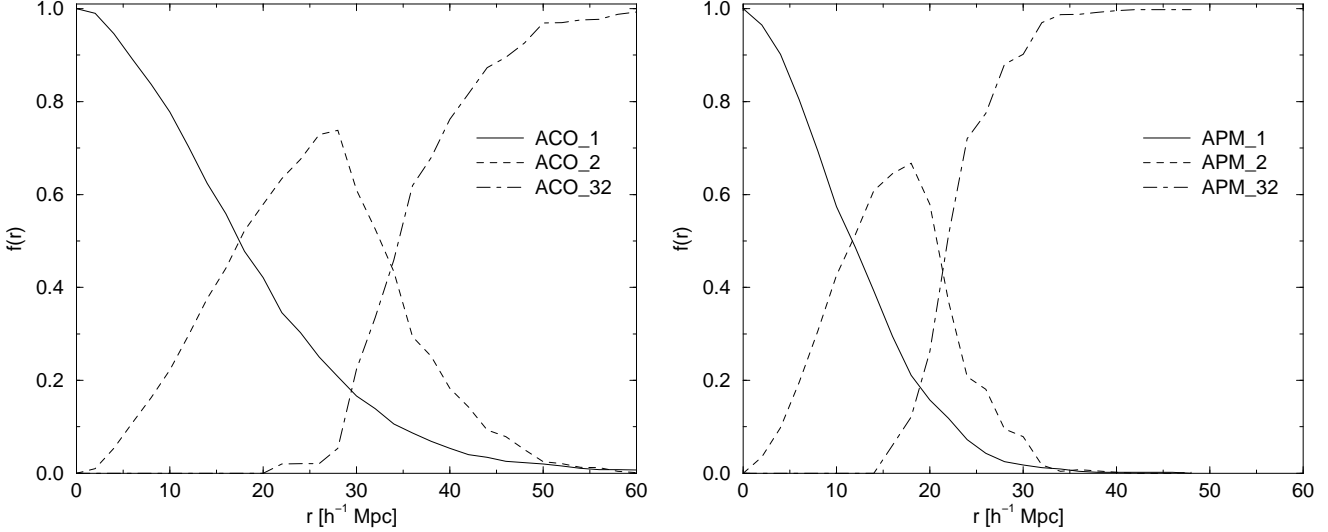


FIG. 5.— Multiplicity functions for ACO and APM superclusters. Solid lines show the fraction of isolated clusters ($N_{cl} = 1$) for different neighborhood radii; dashed lines show the fraction of clusters in superclusters of multiplicity $2 \leq N_{cl} \leq 31$; dot-dashed lines indicate the fraction of clusters in extremely rich systems with $N_{cl} \geq 32$.

or clusters with measured redshifts only (“R”); the following number is the minimum richness of superclusters, N_{cl} : samples denoted by “1” include all clusters (including isolated ones, i.e. superclusters of richness $N_{cl} = 1$); samples designated by “4” are for clusters located in rich superclusters which have at least 4 member clusters, $N_{cl} \geq 4$; finally samples designated by “8” include very rich superclusters with at least 8 members, $N_{cl} = 8$. N denotes the number of clusters in samples. In Table 1 we give parameters of the selection functions, which shall be described in Section 5.1. Finally, we give in Table 1 also the correlation length, r_0 .

3. CLUSTERING OF ABELL AND APM CLUSTERS

Galaxies and clusters of galaxies form large systems, called superclusters. We define superclusters as the largest relatively isolated density enhancements in the Universe, which contain at least one rich cluster of galaxies. An example of a nearby supercluster that contains only one rich cluster is the Local Supercluster. Redshift data on individual galaxies become incomplete at large distances, thus superclusters, as indicators of high-density regions of the Universe, are usually found on the basis of only cluster data.

3.1. Superclusters as defined by Abell and APM clusters

The method to construct a supercluster catalog has been described in detail by EETDA, E97d, and in Paper I. To find high-density regions from cluster data we use the friends-of-friends algorithm. Clusters are assigned to superclusters using a certain neighborhood radius, such that all clusters in the system have at least one neighbor at a distance not exceeding this radius. This neighborhood radius to collect clusters to superclusters should be chosen in accordance with the spatial density of the cluster sample as follows. In Figure 5 we show the fraction of clusters in superclusters of different multiplicity for a wide range of neighborhood radii. At small radii all clusters are isolated, i.e. they belong to superclusters of multiplicity $N_{cl} = 1$. With increasing neighborhood radius some clusters form superclusters of intermediate richness; $2 \leq N_{cl} \leq 32$. At still larger radii (of $15 - 25 h^{-1}$ Mpc) extremely large superclus-

ters with multiplicity $N_{cl} \geq 32$ start to form. By further increasing the neighborhood radius to $\approx 30 h^{-1}$ Mpc, superclusters begin to join into huge conglomerates; finally, at the “percolation radius” of $\approx 45 h^{-1}$ Mpc all clusters percolate and form a single system penetrating the whole space under study. We want to select superclusters as large as possible, but which are still isolated systems. To obtain superclusters with these properties we must choose a neighborhood radius well below the percolation radius. The appropriate neighborhood radius is the radius which corresponds to the maximum of the fraction of clusters in systems of intermediate richness. At this radius very large systems just start to form, as seen from Figure 5 (see also EETDA, E97d and Paper I).

The spatial density of APM clusters is about three times that of Abell clusters (section 5.2, see also Dalton et al. 1992, Croft et al. 1997). This property is reflected in the multiplicity function: these functions are similar for the APM and Abell clusters, but for the APM sample they are shifted to smaller neighborhood radii with respect to those for the Abell sample. For the Abell cluster sample we chose a neighborhood radius of $24 h^{-1}$ Mpc to derive a supercluster catalog, while the APM supercluster catalog was based on a radius of $16 h^{-1}$ Mpc. Both values were chosen so as to maximize the fraction of systems of intermediate richness. The most recent Abell supercluster catalog (as presented in Paper I) is based on all clusters up to a limiting redshift of $z_{lim} = 0.13$. The supercluster catalog based on APM clusters is given in the Appendix of the present paper.

3.2. The distribution of clusters in rich superclusters

Now we shall compare the spatial distribution of superclusters based on the Abell and APM cluster samples. We restrict our comparison to the area of the sky covered by the APM sample. We use supercluster catalogs constructed for all clusters (including clusters with estimated redshifts). We show the distribution of clusters only in superclusters of richness 4 and higher. This has two reasons. First, the

Parameters of selection functions

Sample	N_{cl}	N	$\sin b_0$	d_{0N}	d_{1N}	d_{0S}	d_{1S}	r_0
ACO.A1	1	1663	0.20	0.90	0.34	1.00	0.38	16
ACO.A4	4	741	0.30	0.80	0.35	1.00	0.50	36
ACO.A8	8	373	0.40	0.80	0.50	1.00	0.62	50
ACO.R1	1	1071	0.35	0.90	0.70	1.00	0.80	20
ACO.R4	4	468	0.35	0.80	0.60	1.00	0.80	46
ACO.R8	8	253	0.40	0.80	0.70	1.00	0.90	52
					f_0	r_{min}	r_{max}	
APM.A1	1	939	0.30		1.00	50	310	13
APM.A4	4	427	0.30		1.00	100	310	33
APM.A8	8	240	0.30		1.00	150	310	49
APM.R1	1	356	0.30		0.70	50	190	22
APM.R4	4	159	0.30		0.70	100	190	41
APM.R8	8	95	0.30		0.70	150	170	59

skeleton of the supercluster-void network is essentially determined by rich superclusters; poorer systems only add some fine details to the structure (E97d). Redshift errors do not affect the sky positions of the clusters but have an effect on their radial distance only. Redshift errors have the same effect for superclusters as the velocity dispersion of galaxies in clusters: they elongate the superclusters in the radial direction. This effect may destroy real superclusters, if the separation between individual clusters in the radial direction, due to errors, is too large. Using rich and very rich superclusters we have a higher probability to select real superclusters since it is very unlikely that errors bring isolated clusters together to form compact rich systems.

Figure 3 shows that in this region of the sky the distribution of clusters has two maxima, located at distances $r \approx 200$ and $300 h^{-1}$ Mpc from us. The APM supercluster catalog contains no rich superclusters at distances less than $150 h^{-1}$ Mpc, so we plot in Figure 6 clusters in rich and very rich superclusters in two layers, $150 \leq r < 250 h^{-1}$ Mpc, and $250 \leq r < 350 h^{-1}$ Mpc, which correspond to maxima of the cluster sample density. The richest superclusters in the nearer sheet (lower panels in Figure 6) are the Pisces-Cetus, Grus-Indus, Horologium-Reticulum (see also Park & Lee 1998) superclusters located at RA $\approx 0.1 rad$, $\sin(DEC) \approx -0.4$; RA ≈ -0.6 , $\sin(DEC) \approx -0.8$, and RA ≈ 0.9 , $\sin(DEC) \approx -0.8$, respectively. The richest superclusters in the farther sheet (upper panels) are the Sculptor supercluster at RA ≈ 0.1 , $\sin \delta \approx -0.5$, and the Caelum and Fornax-Eridanus supercluster complex at RA ≈ 1.1 , $\sin \delta \approx -0.6$. Very rich superclusters are seen in both (the Abell and APM) supercluster catalogs based on all clusters, although individual clusters differ.

Extra-large open circles in Figure 6 mark the centers of

very rich superclusters as determined from positions of their member clusters in the APM.R8 supercluster catalog. In the nearer sheet only the Horologium-Reticulum supercluster complex has a sufficient number of members with measured redshifts, and is split into two subsystems, separated by $25 h^{-1}$ Mpc in 3-D space. In the farther sheet we see the Sculptor supercluster which is also split into two subsystems (separated by $50 h^{-1}$ Mpc in 3-D space, see Figure 9). We conclude that the whole APM supercluster catalog, derived on the basis of measured redshifts, is dominated by two very rich supercluster complexes, the Horologium-Reticulum and the Sculptor superclusters. Other rich superclusters in the APM sample have only a few, if any, clusters with measured redshifts. These dominant rich superclusters surround the Sculptor void, one of the largest voids known with a diameter of about $185 h^{-1}$ Mpc. On the borders of this void there are several APM clusters forming a cluster filament. The spatial density of this filament is, however, lower than the minimum density below which for clarity we omit clusters in low-density environments in Figure 6.

The sample of all APM clusters (APM.A1) reaches its maximal spatial density at a distance $r \approx 300 h^{-1}$ Mpc (see Figure 3). It is interesting to note that clusters which belong to rich and very rich superclusters of the APM supercluster catalog (upper right-hand panel of Figure 6) form a quasi-regular pattern on the sky with a period of about 0.4 radians along the RA axis. At a distance of $300 h^{-1}$ Mpc this period corresponds to a linear separation of $\approx 120 h^{-1}$ Mpc. As the sky positions of superclusters are not affected by distance errors, this period cannot be much in error. We see that the whole APM cluster catalog gives a visual impression of a supercluster-void network

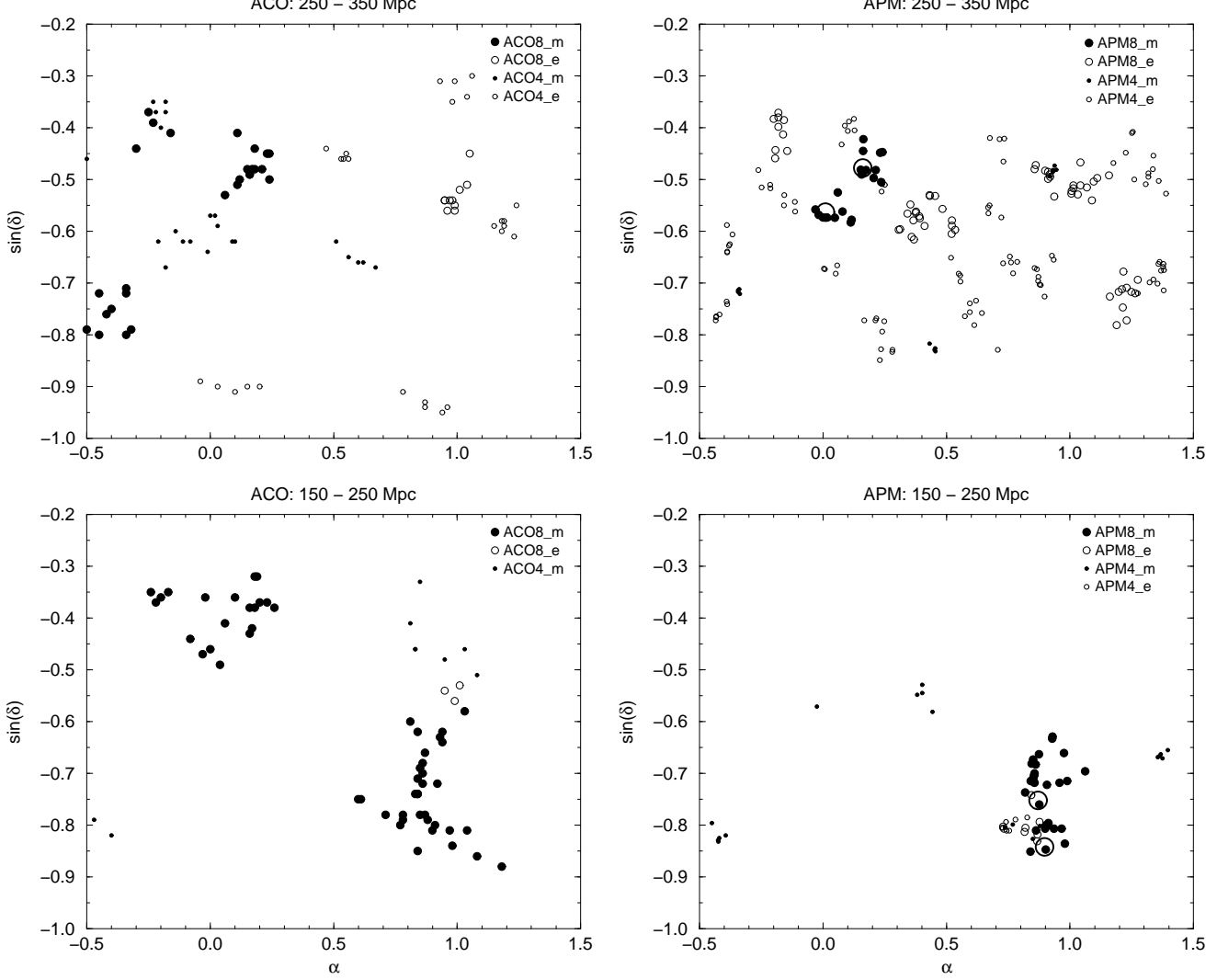


FIG. 6.— The distribution of Abell clusters (left-hand panels) and APM clusters (right-hand panels) in rich and very rich superclusters in equatorial coordinates (RA is given in radians, in vertical axis we plot $\sin \delta$, both for equinox 1950). Large symbols mark very rich superclusters ($N_{cl} \geq 8$), small symbols clusters in superclusters of intermediate richness ($4 \leq N_{cl} < 8$); open symbols are for clusters with estimated, filled symbols for measured redshifts. The upper panels plot clusters in distance interval $250 \leq r < 350 h^{-1}$ Mpc, while the lower panels in interval $150 \leq r < 250 h^{-1}$ Mpc. Centers of very rich superclusters determined from the APM.R8 cluster sample are shown by extra-large open circles.

with a characteristic scale of $\approx 120 h^{-1}$ Mpc between high-density regions, similar to the scale found on the basis of Abell clusters (EETDA, E97d).

4. QUANTITATIVE MEASURES OF CLUSTERING OF ABELL AND APM CLUSTERS

4.1. Correlation functions

The correlation functions were calculated using the classical method:

$$\xi(r) = \frac{\langle DD(r) \rangle}{\langle RR(r) \rangle} \frac{n_R^2}{n^2} - 1, \quad (1)$$

where $\langle DD(r) \rangle$ is the number of pairs of clusters in the range of separations $r \pm dr/2$, dr is the bin size, $\langle RR(r) \rangle$ is the respective number of pairs in a Poisson sample of points, n and n_R are the mean number densities of clusters in respective samples, and brackets $\langle \dots \rangle$ mean ensemble average. The summation is over the whole volume under study, and it is assumed that the cluster and Poisson samples have identical shape, volume and selection functions. No weights are used; the selection effects are applied to Poisson samples and all real and simulated points are treated with equal

weights. The mean error (determined by cosmic variance of samples) was calculated using the equation:

$$\sigma_{\xi_c} = \frac{b}{\sqrt{N}}, \quad (2)$$

where N is the number of clusters in the sample, and $b = 1.5$ is a parameter that describes the character of the large-scale distribution of objects studied (E97b, E97c).

Correlation functions were calculated for all Abell and APM cluster subsamples listed in Table 1. These functions are determined basically by the distribution of clusters which belong to rich and very rich superclusters (E99a). To show the properties of the distribution of high-density regions we plot in Figure 7 correlation functions of clusters in very rich superclusters, samples ACO.A8, ACO.R8, APM.A8 and APM.R8. To generate comparison Poisson samples we used selection functions described in section 5.1 below, with parameters given in Table 1. For samples ACO.R8 and APM.R8 we plot values of the correlation function with error bars, for samples ACO.A8 and APM.A8 we show correlation functions smoothed with Gaussian window of dispersion $10 h^{-1}$ Mpc.

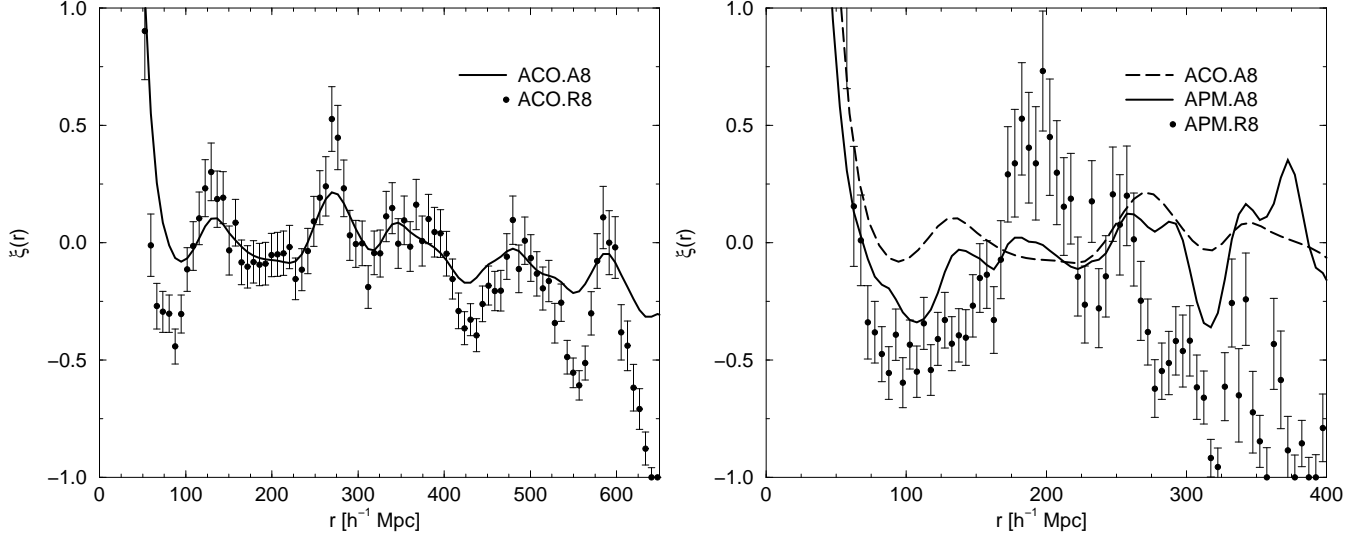


FIG. 7.— The correlation functions of clusters in very rich superclusters for Abell (left hand panel) and APM samples (right-hand panel). Solid lines show correlation functions of all clusters located in very rich superclusters (samples ACO.A8 and APM.A8); dots with error bars designate correlation functions on the basis of cluster samples with measured redshifts (samples ACO.R8 and APM.R8). In the right-hand panel the dashed line marks the correlation function of ACO.A8 clusters for comparison.

Abell clusters occupy a double-conical volume with full depth of $700 h^{-1}$ Mpc, thus it is possible to calculate the correlation function for large separations. The APM sample is defined in a smaller volume, and the correlation function can be found for smaller separations. We see that correlation functions, derived for Abell clusters in very rich superclusters, are oscillating. We can recognize 5 secondary maxima and 6 minima. The mean separation of maxima and of minima is $116 \pm 21 h^{-1}$ Mpc. The differences between correlation functions derived for all clusters and for clusters with measured redshifts (samples ACO.A8 and ACO.R8, respectively) are small.

The correlation function of APM clusters has a more complicated behavior. If we use all clusters (sample APM.A8), then the first and the second secondary maxima have locations close the locations of respective maxima found for Abell cluster samples. Similarly we can identify the first and the third minima with minima in the Abell cluster correlation function. But instead of the second minimum near separations of $r \approx 200 h^{-1}$ Mpc, the APM sample has a maximum at this separation, not present in the Abell sample. If we use only clusters with measured redshifts (sample APM.R8), then the first secondary maximum of the correlation function at $r \approx 130 h^{-1}$ Mpc disappears, and the peculiar maximum at $r \approx 185 h^{-1}$ Mpc has an enhanced amplitude.

The reason for such peculiar behavior can be understood when we consider the distribution of very rich superclusters in the APM samples. The sample with all clusters (APM.A8) is dominated by numerous very rich superclusters located in the more distant shell (see right-hand upper panel of Figure 6). These superclusters are distributed fairly regularly and form a supercluster-void network with a step around $120 h^{-1}$ Mpc (see previous Section). If we use the sample with measured redshifts only (APM.R8) instead, then the number of very rich superclusters in the sample decreases; the sample is dominated by two very rich superclusters that border the Sculptor void, one of the largest voids known (see the extra-large circles in the right panels

of Figure 6 and a jump at $200 h^{-1}$ Mpc of distance distribution of APM.R8 clusters in Figure 9). The secondary maximum of the correlation function of the sample APM.R8 is determined by mutual separations of clusters belonging to these superclusters. We shall discuss this behavior of the APM sample below.

We also calculated the correlation length (i.e. the separation at which the correlation function equals unity), r_0 , for all samples. The results, given in Table 1, show that there are only minor differences between Abell and APM cluster samples. In both cases the correlation length, determined for all clusters, is $r_0 = 18 \pm 3 h^{-1}$ Mpc; for clusters in rich superclusters it is $r_0 = 39 \pm 5 h^{-1}$ Mpc, and for clusters in very rich superclusters, $r_0 = 52 \pm 7 h^{-1}$ Mpc (the mean and scatter are determined from all Abell and APM samples with respective N_{cl}). Similar values have been found by E97b.

4.2. Power spectra

The power spectrum, $P(k)$, is the the Fourier transform of the correlation function, $\xi(r)$, and vice versa:

$$P(k) = 4\pi \int_0^\infty \xi(r) r^2 \frac{\sin kr}{kr} dr; \quad (3)$$

$$\xi(r) = \frac{1}{2\pi^2} \int_0^\infty P(k) k^2 \frac{\sin kr}{kr} dk. \quad (4)$$

here the wavenumber k is measured in units of $h \text{ Mpc}^{-1}$, and is related to the wavelength by $\lambda = 2\pi/k$. Practical procedures to calculate integrals (3) and (4) are given by Press et al. (1992). The Fourier transform yields accurate results only if the correlation function (or the power spectrum) has no errors, and if the power spectrum and the correlation function are given for the whole k or r space, respectively. These conditions are not fulfilled in the case of the real samples. The power spectrum is, by definition, a non-negative quantity. Integral (4) yields for all non-negative power spectra a physically reasonable correlation function, but not all correlation functions submit non-negative results

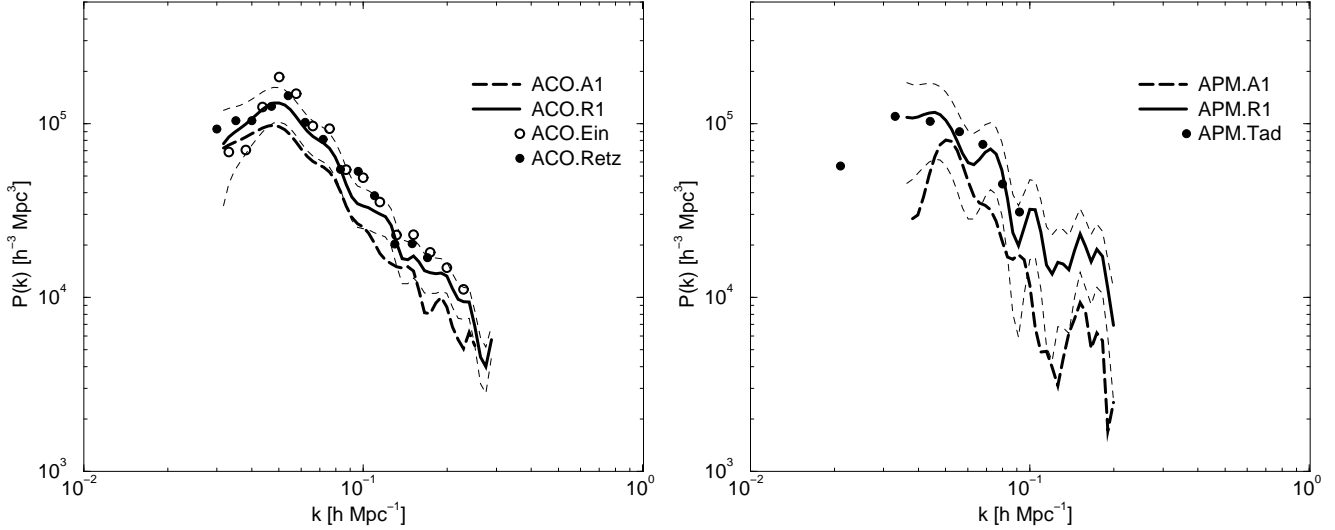


FIG. 8.— Power spectra of ACO (left) and APM clusters of galaxies (right panel). Different symbols are used for spectra based on all clusters and for spectra derived for samples of clusters with only measured redshifts. The error corridor shown for spectra based on samples ACO.R1 and APM.R1 was calculated from the 3σ error of the correlation function. For comparison we show also spectra found by E97a and R98 for Abell clusters, and by T98 for APM clusters.

when one is calculating the power spectrum using formula (3). For this reason random and systematic errors of the correlation function can result non-physical values for the power spectrum.

The most serious systematic error introduced by the cluster correlation function is due to the peculiar shape of cluster samples. The correlation function of clusters in superclusters has an oscillatory behavior: at large separations it contains regularly spaced secondary maxima and minima. Maxima correspond to mutual separations between rich superclusters, and minima to mean separations of voids. If the sample occupies fully a large truly 3-D volume, then the amplitude of oscillations of the correlation function decreases almost exponentially, since on large separations rich superclusters located in different directions reduce the maxima and minima of the correlation function (see E97c for a discussion). If the sample volume is not fully 3-dimensional, then the cancellation is less effective. In the extreme case, if the sample is given in a cylindrical (essentially one-dimensional) volume, and if superclusters are regularly spaced along the axis of the sample, then the amplitude of oscillations of the correlation function does not decrease with increasing separation of superclusters. If we take a double-conical volume, as is the actual Abell sample volume that contains no clusters near the Galactic equator, then the cancellation of maxima and minima is partial. In a sample of such elongated form the amplitude of oscillations of the correlation function decreases with the increase of the separation more slowly than in the case of a fully 3-D sample.

To correct for such an effect we have to suppress the amplitude of oscillations of the correlation function on large separations, preserving the shape of the function on small separations. Our experience has shown that an appropriate correction can be achieved if we multiply the observed correlation function by a factor $\exp(-r/r_c)^2$, here r_c is a parameter. We have checked the recovery procedure using correlation functions found via (4) from analytical power spectra, distorted to increase the amplitude of oscillations,

and thereafter corrected according to the procedure outlined above. This trial has shown that this procedure recovers the actual shape of the power spectrum rather closely. By a trial-and-error procedure we have found that a value $r_c = 150 h^{-1}$ Mpc yields best recovery of analytical and observed correlation functions.

We have investigated also the influence of random errors on the correlation function. We added random noise to the distorted correlation function; this noisy correlation function was reduced using the procedure given above, and Fourier-transformed to obtain the recovered power spectrum. This test has shown that purely random errors have little influence. Actually random, systematic (due to sample shape) and cosmic (deviations of samples found for limited volume from the underlying large parent sample) errors distort observed correlation functions in a more complicated way. Thus the recovered power spectrum may still have some further peculiarities.

The power spectra of ACO and APM cluster samples found on the basis of their correlation functions are shown in Figure 8. Here we have used correlations functions of all clusters and of clusters with measured redshifts only, samples ACO.A1, ACO.R1, APM.A1, and APM.R1. Our experience has shown that our recovery procedure yields for real cluster samples meaningful results only in the wavenumber interval $0.03 - 0.04 \leq k \leq 0.2 - 0.3 h \text{ Mpc}^{-1}$. On smaller scales the power spectrum is noisy and contains sections with negative values, on larger scales the error corridor found on the basis of the error corridor of the correlation function becomes very large. For both cluster samples the amplitude of the power spectrum for all clusters is lower than for clusters with measured redshifts. This is probably due to observational errors which smooth the structure and reduce the amplitude of density perturbations. The shape of the power spectra for samples ACO.A1 and ACO.R1 is very similar. In contrast, the position of the maximum of the power spectrum of samples APM.A1 and APM.R1 is different: for APM.A1 it lies at $k \approx 0.05 h \text{ Mpc}^{-1}$, similar to the maximum of Abell cluster samples, whereas for

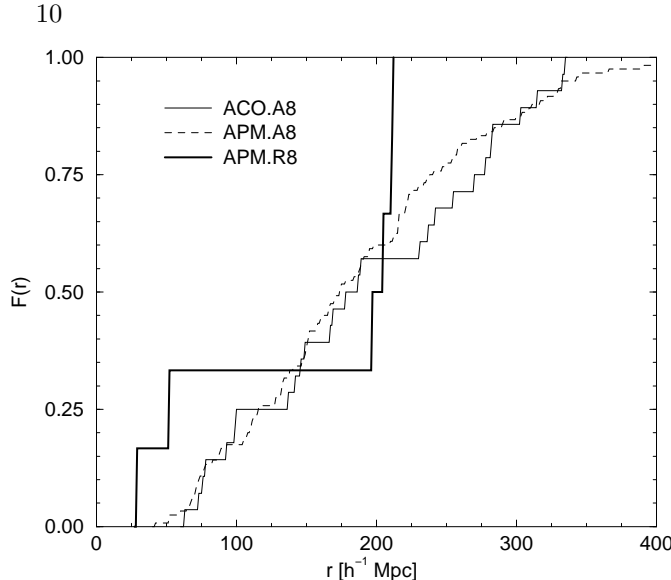


FIG. 9.— Cumulative distribution of distances between centers of superclusters for Abell and APM very rich superclusters. Only Abell superclusters in the APM window were considered.

APM.R1 it lies at $k \approx 0.04 h \text{ Mpc}^{-1}$. This difference is due to differences in correlation functions, compare with Figure 7.

4.3. The distribution of distances between superclusters

So far we have characterized the distribution of clusters using the correlation function and its Fourier transform, the power spectrum. An additional measure is the distribution of distances between superclusters. While correlation functions and power spectra were calculated on the basis of cluster samples, we now consider the distribution of centers of superclusters. Our main goal is to find the reason why the secondary maximum of the correlation function for the sample APM.R8 is shifted towards larger separations compared to results obtained with Abell cluster and APM.A8 samples. As these functions are basically determined by the distributions of high-density regions, we shall derive the distribution of mutual distances of very rich superclusters with at least 8 members. For this we use the samples APM.A8 and APM.R8. For comparison we also derive the distribution of distances between Abell superclusters (ACO.A8) located in the region of sky covered by the APM cluster sample. Integrated distributions of distances are shown in Figure 9.

We see that there are practically no differences between the distribution of distances of Abell and APM superclusters, at least if we use superclusters based on samples including all clusters. This result confirms our earlier findings, based on the correlation function, that Abell and APM samples of all clusters have similar clustering properties. In contrast, the distribution of distances between rich superclusters, found for APM clusters with measured redshifts, is very different. The APM.R8 supercluster sample contains only two supercluster complexes, the Horologium-Reticulum supercluster and the Sculptor supercluster located on opposite sides of the Sculptor void (Figure 3). By chance this is the largest cluster-defined void in our vicinity. These very rich systems have the strongest effect on the correlation function of APM clusters with measured redshifts. The distances between these superclusters characterize the size of the Sculptor void between them, $185 h^{-1} \text{ Mpc}$ (the

distances between supercluster centers are slightly larger, about $200 h^{-1} \text{ Mpc}$). As we have shown above, the correlation function of APM clusters with measured redshifts has its secondary maximum exactly at the same distances. Thus, this maximum in the correlation function is due to the mutual separation of these two superclusters. For comparison: the new Abell cluster sample contains 31 very rich superclusters (see Table A1 in Paper I) and 16 voids cataloged by EETDA and surrounded by rich superclusters. To summarize: the Abell cluster sample (and partly also the APM sample of all clusters) characterizes mean properties of the supercluster-void network, whereas the APM sample with measured redshifts reflects properties of an extremely large deviation from the mean.

5. DISCUSSION

In this section we discuss differences observed between two catalogs of clusters, and between statistics derived from these catalogs in more detail. We shall concentrate on two aspects of the problem: the selection function, and the correlation function. Thereafter we shall compare both cluster samples for their capabilities in tracing the supercluster-void network.

5.1. Selection effects in Abell and APM cluster samples

Suppose that we study a certain volume in the Universe and have in this volume a parent sample of clusters of galaxies. Let $N_{\text{true}}(V, \mathcal{R})$ be the actual number of clusters in this volume, V , with a true limiting number of galaxies in the cluster, \mathcal{R} , varying from cluster to cluster. Galaxies are chosen within a projected distance of one Abell radius ($1.5 h^{-1} \text{ Mpc}$) around the cluster center, and no more than 2 magnitudes fainter than the 3rd-brightest galaxy. This working definition was used by Abell (1958) and ACO. The cluster richness was then determined from the resulting number of galaxies counted in a circle of angular radius based on an assumed cluster distance, which was estimated from the apparent magnitude of the 10th-brightest galaxy. All quantities used in the cluster definition are subject to random and systematic errors; thus the observed number of

clusters, $N_{obs}(V, \mathcal{R})$, differs from the true one. In general, the numbers of observed and true clusters of galaxies are related as follows:

$$N_{obs}(V, \mathcal{R}) = \Phi(V, \mathcal{R}) N_{true}(V, \mathcal{R}), \quad (5)$$

where

$$\Phi(V, \mathcal{R}) = \prod \varphi_i(V, \mathcal{R}), \quad (6)$$

and $\varphi_i(V, \mathcal{R})$ are probabilities to detect a cluster of richness \mathcal{R} in the volume V , given the various selection effects, and the errors in the parameters used in the cluster definition. Here we assume that selection effects and errors i are independent of each other. Most selection effects decrease the number of observed clusters, i.e. the respective probabilities are $\varphi_i \leq 1$. Errors in parameters of cluster definition have various effect; they may both decrease and increase the probabilities φ_i .

Now we consider the effects of selection and errors in more detail. One well-known error is the one in background subtraction. Every cluster is located in a certain environment; thus the observed number of galaxies in a given cluster has to be corrected for the expected number of background galaxies. Remember that Abell (1958) estimated a local background for each cluster, while ACO used an universal luminosity function. This correction is subject to errors: in a high-density environment the background may increase the observed cluster richness \mathcal{R} so that a poor cluster with $\mathcal{R} < \mathcal{R}_0$ is observed as $\mathcal{R} \geq \mathcal{R}_0$. Here \mathcal{R}_0 is the minimal richness of the cluster to be included in the catalog; for Abell clusters of richness class 0 $\mathcal{R}_0 = 30$. This systematic effect is enhanced in superclusters where clusters are affected not only by the universal background but also by overlapping clusters. This effect is detected in the Abell catalog; it makes the two-dimensional correlation function (calculated for different radial and angular separations) elongated in the radial direction and increases the correlation length (Sutherland 1988). To avoid such a systematic error the background correction was made very carefully for the APM cluster catalog (D97). Since the background correction is always influenced by random errors, the true minimal number of galaxies in clusters \mathcal{R}_{0t} fluctuates around the accepted number \mathcal{R}_0 .

Another well-studied selection effect is the dependence of the observed number of clusters on Galactic latitude, b . Usually this effect has been taken into account only by exclusion of clusters at low Galactic latitudes, $b \leq 30^\circ$ (Sutherland 1988). Our analysis has shown that actually the spatial density of clusters is an almost linear function of $\sin b$, even at $|b| > 30^\circ$. This dependence can be described through the probability function:

$$\varphi_b = \begin{cases} 0, & \sin b \leq \sin b_0; \\ \frac{(\sin b - \sin b_0)}{(1 - \sin b_0)}, & \sin b > \sin b_0; \end{cases} \quad (7)$$

here $\sin b_0$ is the value of $\sin b$ where the density of clusters reaches zero. Such a dependence was found by E97b, E97d, and in Paper II, and is confirmed by the present study. For Abell and APM cluster samples investigated in this study the values of the parameter $\sin b_0$ are given in Table 1. The latitude dependence can be considered as a random exclusion of faint and/or low surface brightness galaxies from clusters, so that the number \mathcal{R} decreases and a cluster may

fall below the limiting number \mathcal{R}_l , so that the cluster is not included to the catalog. From statistical point of view clusters are included to the catalog only with a certain probability which decreases with the increase of angular distance from Galactic pole. This process decreases also the number of clusters in superclusters; thus the density of clusters in rich superclusters decreases with decreasing Galactic latitude more rapidly than the density of all clusters. This dependence can be modeled using mock samples; random exclusion model with probability function (5) describes well the latitude distribution of clusters in superclusters of various richness (E97c).

The third selection effect is the dependence of the number of observed clusters on the distance from the observer. The mean density is usually found by appropriate smoothing of the observed number of clusters as a function of z (Efstathiou et al. 1992, Croft et al. 1997). The distance dependence of the spatial density of the cluster sample is due to several different effects. One effect is related to the difficulty to detect, especially a poor cluster, on large distances. Secondly, nearby clusters cover too large an area on the sky to use standard cluster searching algorithm, and are thus omitted. Further, near the limit of the sample errors of the estimated redshift influence the completeness of the sample. And finally, far from all clusters have their redshifts measured.

The physical background of the difficulty to find a distant cluster is not clear, but probably it is due to detection problems of galaxies of low surface brightness at large distance. This reduces the number of galaxies found in the cluster below the threshold of \mathcal{R}_0 . A similar detection problem may be the reason for the latitude dependence of the spatial density of clusters. Formally this selection effect can be modeled as a random exclusion of clusters from a general sample of true clusters. Following E97b and E97d, we use the linear probability function:

$$\varphi_{r1}(r) = d_0 - d_1 \frac{r}{r_{lim}}, \quad (8)$$

where d_0 is the probability to detect a cluster in our vicinity ($r = 0$); $d_0 - d_1$ is the probability to detect a cluster at distance r_{lim} ; and r_{lim} is the limiting radius of the sample. We adopt $d_0 = 1$ for the southern part of the Abell sample. Table 1 lists the parameters d_0 and d_1 for northern and southern Abell cluster samples.

The second distance-dependent selection effect is due to random errors of estimated redshifts. Clusters near the far limit of the sample are selected by the following criterion: both the Abell and APM samples have been selected using an upper limit for the estimated redshift, z_{lim} . Estimated redshifts are subject to random errors, with approximately log-normal distribution of dispersion 1.3 in $\log z$ (see Figure 2). This effect causes a deficit of clusters near the limit $z \leq z_{lim}$. On the other hand, some clusters within the limit z_{lim} have true redshifts exceeding the estimated one, thus the density distribution has a large tail of clusters with $z_{meas} > z_{lim}$ but $z_{est} < z_{lim}$. To decrease this distance selection effect we apply for the Abell sample an upper limit for the estimated redshift, $z = 0.15$, which exceeds by $\Delta z = 0.02$ the redshift limit of the sample used for our structure analysis, $z_{lim} = 0.13$. Figure 3 shows that a rapid decrease of the spatial density of clusters near the

limit of the sample can be avoided by this procedure. A similar cut would limit the APM sample to $z_{lim} = 0.10$. Instead we applied an identical cut for both cluster samples, $r_{lim} = 350 h^{-1}$ Mpc, at the cost of introducing this selection effect in the APM sample. The rapid decrease of the density of APM clusters beyond $300 h^{-1}$ Mpc is due to the sharp cutoff of the estimated redshift at $z = 0.118$ or $r = 325 h^{-1}$ Mpc (see Figure 2).

The third distance-dependent selection effect is due to difficulty to detect a very nearby cluster spanning a large area on the sky (D97). This effect is practically absent in the Abell catalog; only the Virgo cluster was excluded from the Abell catalog for this reason. For APM clusters this effect is enhanced by the absence in the APM sample galaxies brighter than $b_j = 17$ (which are overexposed and cannot be measured automatically, see Maddox, Efstathiou & Sutherland 1990). Due to this selection effect the APM cluster sample is very sparse at small distances of $r < 100 h^{-1}$ Mpc from us; this explains also the absence of nearby rich superclusters in the APM sample, (see Figure 3).

So far we have discussed selection effects in samples of all clusters. As not all clusters have a measured redshift, another distance-dependent selection effect occurs in samples of clusters with only measured redshifts. The overall distance-dependent selection probability was calculated by Efstathiou et al. (1992) and Croft et al. (1997) by smoothing the observed redshift distribution. We use a different approach here, and calculate the combined effect of all distance-dependent selection effects for Abell clusters by eq. (6). For the APM cluster samples the combined effect of distance-dependent selections can be approximated by the following law:

$$\varphi_{r2}(r) = \begin{cases} 0, & r \leq r_{min}; \\ f_0 \frac{(r-r_{min})}{(r_{max}-r_{min})}, & r_{min} < r \leq r_{max}; \\ f_0 \frac{(r_{lim}-r)}{(r_{lim}-r_{max})}, & r_{max} < r \leq r_{lim}; \end{cases} \quad (9)$$

here we assume that at a distance r_{max} clusters are detected with a probability f_0 . This probability function was used to calculate the comparison Poisson sample for the APM clusters. Values of the parameters r_{min} , r_{max} , and f_0 are given in Table 1.

We summarize the discussion of selection effects in Abell and APM cluster catalogs as follows. Both cluster catalogs are subject to similar selection effects in Galactic latitude. The error due to overlapping of clusters in superclusters is present only in the Abell catalog. This error may distort the structure of individual superclusters (and the cluster correlation function on small separations). However, it is of less importance for the study of the structure of the supercluster-void network, since it does not decrease systematically the number of clusters in superclusters. Distance-dependent selection effects are rather small in the Abell cluster sample, but very large in the APM sample. We shall discuss the influence of these selection effects on the study of the supercluster-void network in section 5.5 below.

5.2. Spatial density and volume covered by the Abell and APM cluster samples

In order to calculate the spatial density of Abell and APM clusters of galaxies we generate Poisson samples with selection function parameters as given in Table 1. We count the total number of particles, and the number of particles left after the selection functions have been applied. We obtain $\rho = 27.6 \times 10^{-6} h^3$ Mpc $^{-3}$ for the ACO.A1 sample and $\rho = 83 \times 10^{-6} h^3$ Mpc $^{-3}$, for APM.A1. Our value for Abell clusters confirms earlier density estimate by E97d, but is about twice the value found by Bahcall & Cen (1993). The reason for this discrepancy is our more detailed account of the selection function (see eq. (7)).

The surface of the sky covered by the sample of Abell clusters, can be estimated, when we fix the effective Galactic latitude limit of the survey. The large-scale distribution of high-density regions can be investigated if superclusters of richness $N_{cl} \geq 4$ are included in the sample (E97d). Figure 4 shows that the density of clusters in rich superclusters drops to zero at $\sin b \approx 0.30$. Thus we find that the Abell cluster survey covers 8.8 steradians (sr) on the sky. The APM survey is limited by $-0.30 \geq \sin \delta \geq -0.95$ in declination and $\Delta RA = 130^\circ$ in right ascension, corresponding to an area of 1.47 sr. The volume occupied by the Abell sample ACO.A1 is $126 \times 10^6 h^{-3}$ Mpc 3 . The depth of the APM sample is from $50 h^{-1}$ Mpc to $350 h^{-1}$ Mpc, corresponding to a volume of the APM survey $21 \times 10^6 h^{-3}$ Mpc 3 . Here we are speaking on the volume of the *sample* of Abell or APM clusters, not the volume occupied by Abell or APM clusters themselves.

We can also find the effective volume of both samples, defined by the number of clusters in the sample divided by the mean density (we mean the true mean density which is calculated after the correction for all selection effects). We get $60 \times 10^6 h^{-3}$ Mpc 3 and $11 \times 10^6 h^{-3}$ Mpc 3 , for the ACO.A1 and APM.A1 samples. The effective volumes of samples ACO.R1 and APM.R1 are even less, $40 \times 10^6 h^{-3}$ Mpc 3 and $5 \times 10^6 h^{-3}$ Mpc 3 , respectively. We see that the selection effects reduce the effective volume with respect to the actual volume of samples. Volume estimates show that the APM sample of all clusters occupies a volume about 1/6 of the volume of the corresponding Abell sample ACO.A1. The volume estimate given by T98 is larger than found in the present paper, since T98 also included regions where the sample is very sparse.

5.3. Correlation functions

The cluster correlation function has been a subject of intensive studies starting from the pioneering work by Klypin & Kopylov (1983) and Bahcall & Soneira (1983). In most cases the main purpose was the determination of the correlation length, r_0 , and the power index, γ , of the function; for recent studies we refer to Sutherland (1988), Efstathiou et al. (1992), Dalton et al. (1992), and Croft et al. (1997). These authors have shown that the correlation length for APM clusters is smaller than that for Abell clusters. This can be explained in part by the overlapping of Abell clusters in superclusters; a small intrinsic difference is also possible. As shown by real data and numerical simulations, the cluster correlation function depends on cluster richness (Bahcall & West 1992, Bahcall & Cen 1992, Frisch et al. 1995). We also find a weak difference of the cluster correlation length for Abell and APM samples. A much stronger dependence exists for clusters located in different environments: the

correlation length for clusters in rich and very rich superclusters is much higher than for all clusters (E97b, Paper II). This effect is due to variable density threshold in the definition of clusters in a different environment, for an analysis of this effect see Einasto et al. (1999b). In the present study we confirm this result (see Table 1): *there is no unique value of the cluster correlation length – it depends on cluster richness and environment.*

In the present study we have concentrated on the study of cluster correlations at large separations. For small separations the correlation function characterizes the distribution of clusters in superclusters, and for large separations the distribution of superclusters themselves, i.e. properties of the supercluster-void network (E97c). The present study has confirmed earlier findings of E97b, that on large scales the Abell cluster correlation function is oscillating, i.e. it consists of alternating secondary maxima and minima. Oscillations are clearly detected if we use samples of clusters in very rich superclusters. There is practically no difference between the oscillatory behavior of samples of all clusters and clusters with measured redshifts, ACO.A8 and ACO.R8, respectively. We find a period of oscillations of $116 \pm 20 h^{-1}$ Mpc, very close to the value found earlier. The APM cluster sample also shows signs of oscillations with the same period, if we use all clusters (sample APM.A8). If we use clusters with measured redshifts only (sample APM.R8), we see again a strong secondary maximum, but at much larger separation corresponding to the mutual distance of two dominating superclusters in the sample, the Horologium-Reticulum and the Sculptor superclusters (see Figure 6). This is the main difference between Abell and APM samples of clusters. We continue the discussion of this difference in the next Section.

5.4. Abell and APM clusters as tracers of the supercluster-void network

The principal statistic to characterize the distribution of matter on large scales has been the power spectrum of clusters of galaxies. Our study confirms previous evidence (E97a, R98, and T98) for the existence of a real differences between power spectra of Abell and APM cluster samples. The power spectrum of the Abell sample has a peak on a scale of $\approx 120 h^{-1}$ Mpc. A peaked power spectrum corresponds to an oscillating correlation function (E97a) with a period of $120 h^{-1}$ Mpc. The APM cluster sample as analyzed by T98 has no feature on this scale. It has been argued that the APM cluster sample is free of the projection and selection biases known to affect the Abell cluster sample (T98). For this reason the reality of the feature seen in the Abell sample has been questioned (Postman 1998). This brings us to the central problem of our study: How well do the Abell and APM cluster samples trace the structure of the Universe on large scales?

Our study has shown that selection effects are more complicated than assumed previously. In particular, the selection function in distance depends on four different effects: the difficulty to detect clusters at large and small distances, the deficiency of clusters at large distance due to random errors in estimated redshifts used for the selection of clusters, and the selection caused by observing programs of cluster redshifts. Our analysis has shown that the sample of all Abell clusters (ACO.A1) is affected by distance-dependent selection effects only on very large distances; this selection

effect may be reduced if the sample is cut at a redshift of $z = 0.13$. In contrast, the APM sample with measured redshifts (APM.R1) is affected by several distance-dependent selection effects within the range of distances of interest for the present study.

T98 has compensated distance-dependent selection effects using weights for clusters inversely proportional to the mean spatial density of the cluster sample at its respective distance, following the prescription by Feldman, Kaiser & Peacock (1994, hereafter FKP). T98 has also applied truncation of the sample at large distances, $r_{lim} = 600$ and $400 h^{-1}$ Mpc. The resulting estimates of the spectrum are similar, but the scatter of the power spectrum is smaller when cutting the sample at smaller distance. T98 argue that the sample of APM clusters with measured redshifts is representative for a volume of depth $400 h^{-1}$ Mpc.

The Figure 3 shows that the spatial density of the APM sample is very low at large distances. The same effect can be seen also in Figure 1 of T98 (note that T98 do not plot the spatial density, but the number of clusters in respective bins). The comparison of the spatial densities of the Abell and APM samples in Figure 3 demonstrates that the APM sample with measured redshifts becomes very sparse or diluted at distances $r > 300 h^{-1}$ Mpc; in the Abell sample dilution becomes strong only at distances $r > 400 h^{-1}$ Mpc. The question is: Is the use of weights sufficient to compensate for the strong dilution observed in the APM sample at large distance?

FKP argue that statistical properties of large scale structures can be fixed by using sparse samples if density perturbations are Gaussian. The Gaussian character of small-scale perturbations has been checked by the analysis of FKP. On large scales the problem is unsolved. Szalay (1998) has demonstrated that the distribution of large structures (supercluster-void network generated by Voronoi tessellation) may be destroyed completely by randomization of the phases of perturbations without changing the power spectrum. A sparse sample cannot distinguish between a regular supercluster-void network and random distribution of high-density regions. This simple example shows very clearly that a very sparse sample is not suitable to describe the real supercluster-void network.

Our experience has shown (Einasto et al. 1991, Frisch et al. 1995, E97c) that dilution is not dangerous to locate high-density regions, as long as the main structural elements are not destroyed. The distribution of matter on large scales is dominated by the supercluster-void network. Thus, in order to investigate the character of the mass distribution on large scales, rich superclusters must be present in sufficient quantities (E97c). Figure 3 shows that the Abell cluster sample is complete enough to trace the network of rich superclusters up to $r_{lim} = 375 h^{-1}$ Mpc. The APM sample with measured redshifts contains only two rich supercluster complexes within a distance of $r = 325 h^{-1}$ Mpc. The mutual separation of these two supercluster complexes determines the shape of the correlation function and the power spectrum of the whole APM sample of clusters with measured redshifts. But this is not sufficient to trace the whole supercluster-void network. The sample is diluted and not all rich superclusters actually present can be traced in this distance range (see Figure 6).

This example shows that the use of the weights does not compensate for the lack of data. The APM sample of all

clusters contains a sufficiently large number of rich and very rich superclusters, but most of the clusters in these superclusters do not yet have measured redshifts. The analysis of the sample of all APM clusters has shown that using this larger sample will probably yield a more representative picture of the supercluster-void network. T98 has used the APM cluster sample B for which a limit of estimated redshifts $z_{est} \leq 0.118$ was applied, corresponding to the apparent magnitude limit of $m_X \leq 19.4$. This limit is implied by the limiting magnitude of the APM galaxy survey, $b_J = 20.5$, and the magnitude range $[m_X - 0.5, m_X + 1.0]$ to determine the cluster richness \mathcal{R} . Croft et al. (1997) have formed a deeper APM cluster sample C, using a fainter limiting magnitude of the galaxy catalog, $b_J = 21.0$, and a narrower magnitude range $m_X - 0.5, m_X + 0.7$, which yields $r_{lim} = 850 h^{-1}$ Mpc for the sample C. This sample contains several rich superclusters at a distance of $\approx 600 h^{-1}$ Mpc; these superclusters are also seen in the Abell catalog as clusters of distance class 6 (Croft et al. 1997). Unfortunately, this much deeper APM cluster sample has not yet been studied to determine the power spectrum.

To conclude the discussion we can say that presently the Abell cluster sample yields more accurate data on the structure of the supercluster-void network than the APM sample with measured redshifts – the effective volume of the last sample is too small.

6. CONCLUSIONS

We have compared the spatial distribution of Abell and APM clusters and cluster-defined superclusters in order to understand the similarities and differences between the correlation functions and power spectra of these clusters. Our main results can be summarized as follows.

1) We have compiled a catalog of superclusters on the basis of APM clusters; the catalog contains data on 55 superclusters with at least 4 members, it is given in Appendix; most clusters have only estimated redshifts.

2) Abell and APM clusters of galaxies show almost identical high-density regions (i.e. rich and very rich superclusters) in the space where samples overlap, if all clusters are used to trace the structure.

3) The sample of APM clusters with measured redshifts covers a much smaller volume in space than that of the Abell clusters. Statistical properties of the APM sample with measured redshifts reflect the distribution of clusters in this particular volume which is dominated by two very rich supercluster complexes. The Abell sample of clusters contains 31 very rich superclusters and can be considered as a candidate of a fair (representative) sample of the Universe.

4) The location of the secondary maximum of the correlation function for APM clusters with measured redshifts at a separation of $r = 185 h^{-1}$ Mpc, and the position of the maximum of the power spectrum, $k = 0.033 h \text{ Mpc}^{-1}$, correspond to the mutual separation between the Horologium-Reticulum and the Sculptor superclusters; and do not characterize the structure of the whole supercluster-void network.

5) The analysis of the new Abell sample of clusters confirms earlier findings that the cluster power spectrum has a maximum on a scale of $k = 0.05 h \text{ Mpc}^{-1}$ which corresponds to the period of the supercluster-void network, $120 h^{-1}$ Mpc.

6) The use of weights in calculation of the correlation function and the power spectrum does not compensate for the lack of data. Properties of the supercluster-void network can only be determined if data are available for a sufficiently large number of rich superclusters.

APPENDIX: APM SUPERCLUSTER CATALOG

The catalog of superclusters of Abell clusters is based on cluster sample ACO.A2, i.e. it contains all superclusters of richness class $N_{cl} \geq 2$. This catalog is published in Paper I.

Here we present a supercluster catalog based on the APM cluster sample used in this paper. The catalog is based on cluster sample APM.A4, i.e. it contains all superclusters of richness class $N_{cl} \geq 4$, the reason of the use of this limit was given above – it is due to the large number of clusters without measured redshifts in the APM sample, thus increasing the limit of member clusters for the catalog we hope to increase the reliability of the catalog. N_{cl} is the number of member clusters in the supercluster; RA_C and δ_C are coordinates of the center of the supercluster (equinox 1950.0), derived from coordinates of individual clusters; D_C is the distance of the center from us; it follows the list of Abell clusters which are members of the supercluster. An index "e" after the Abell or APM cluster number in the column 6 shows that this cluster has estimated velocity. In the last column we list a commonly used name of the supercluster, identifications show the number of corresponding supercluster in the Table A1 of Paper I.

We thank Enn Saar and Alexei Starobinsky for stimulating discussion. This work was supported by the Estonian Science Foundation grant 2625. JE thanks Astrophysical Institute Potsdam for hospitality where part of this study was performed. HA thanks CONACyT for financial support under grant 27602-E.

REFERENCES

Abell, G., 1958, ApJS, 3, 211
 Abell, G., Corwin, H., Olowin, R., 1989, ApJS, 70, 1 (ACO)
 Andernach, H., & Tago, E., 1998, Proc. "Large Scale Structure: Tracks and Traces", eds. V. Müller, S. Gottlöber, J.P. Mücke, & J. Wambsganss, World Scientific, Singapore, p. 147
 Bahcall, N.A., 1988, ARA&A, 26, 631
 Bahcall, N.A., & Cen, R., 1992, ApJ, 398, L81
 Bahcall N.A. & Cen R., 1993, ApJ 407, L49
 Bahcall, N.A. & Soneira, R. 1983, ApJ, 270, 20
 Bahcall, N.A. & West, M., 1992, ApJ, 392, 419
 Broadhurst, T.J., Ellis, R.S., Koo, D.C., & Szalay, A.S. 1990, Nature, 343, 726
 Croft, R.A.C., Dalton, G.B., Efstathiou, G., Sutherland, W.J., & Maddox, S.J., 1997, MNRAS, 291, 305
 Dalton, G.B., Efstathiou, G., Maddox, S.J., & Sutherland, W.J., 1992, ApJ, 390, L1
 Dalton, G.B., Maddox, S.J., Sutherland, W.J., & Efstathiou, G. 1997, MNRAS, 289, 263
 Efstathiou, G., Dalton, G.B., Sutherland, W.J., & Maddox, S.J., MNRAS, 257, 125
 Einasto, J., Einasto, M., Frisch, P., Gottlöber, S., Müller, V., Saar, V., Starobinsky, A.A., Tago, E., Tucker, D., Andernach, H., 1997b, MNRAS, 289, 801, (E97b)
 Einasto, J., Einasto, M., Frisch, P., Gottlöber, S., Müller, V., Saar, V., Starobinsky, A.A., Tucker, D., 1997c, MNRAS, 289, 813, (E97c)

Einasto, J., Einasto, M., Gottlöber, S., Müller, V., Saar, V., Starobinsky, A. A., Tago, E., Tucker, D., Andernach, H., Frisch, P., 1997a, *Nature* 385, 139 (E97a)

Einasto, J., Einasto, M., Gramann, M., & Saar, E. 1991, *MNRAS*, 248, 593

Einasto, J., Einasto, M., Tago, E., Starobinsky, A.A., Atrio-Barandela, F., Müller, V., Knebe, A., Frisch, P., Cen, R., Andernach, H., & Tucker, D., 1999a, *ApJ*, 519, 441

Einasto, J., Einasto, M., Tago, E., Müller, V., Knebe, A., Cen, R., Starobinsky, A.A. & Atrio-Barandela, F., 1999b, *ApJ*, 519, 456

Einasto J., Jöeveer M. & Saar E., 1980, *MNRAS*, 193, 503

Einasto, M., Einasto, J., Tago, E., Dalton, G.B., Andernach, H., 1994, *MNRAS*, 269, 301 (EETDA)

Einasto, M., Einasto, J., Tago, E., Hasinger, G., Müller, V., & Andernach, H. 2001, *ApJ*, submitted (Paper I)

Einasto, M., Tago, E., Jaaniste, J., Einasto, J., Andernach, H., 1997d, *AAS*, 123, 119 (E97d)

Feldman, H.A., Kaiser, N., & Peacock, J.A., 1994, *ApJ*, 426, 23

Frisch, P., Einasto, J., Einasto, M., Freudling, W., Fricke, K.J., Gramann, M., Saar, V., & Toomet, O., 1995, *AA*, 296, 611

Klypin, A.A. & Kopylov, A.A. 1983, *Soviet Astr. Letters*, 9, 41

Maddox, S.J., Efstathiou, G., & Sutherland, W.J. 1990, *MNRAS*, 246, 433

Maddox, S.J., Efstathiou, G., & Sutherland, W.J. 1996, *MNRAS*, 283, 1227

Mattig, W., 1958, *Astr. Nachr.* 284, 109

Miller, C., & Batuski, D., 2000, *ApJ*, submitted [astro-ph/0002295]

Oort, J., 1983, *ARA&A*, 21, 373

Park, C., & Lee, S., 1998, subm. to *J. Korean Astron. Soc.*, [astro-ph/9809372]

Peacock J., & West M.J., 1992, *MNRAS* 259, 494

Press, W. H., Teukolsky, S. A., Vetterling, W. T. & Flannery, B. P., *Numerical recipes in FORTRAN. The art of scientific computing*, Cambridge University Press, 1992, 2nd ed.

Postman, M., 1998, *Evolution of Large Scale Structure: From Recombination to Garching*, eds. A.J. Banday, R.K. Sheth, L.N. da Costa, Garching 1999, p. 270, [astro-ph/9810088]

Retzlaff, J., Borgani, S., Gottlöber, S., Klypin, A., & Müller, V. 1998, *NewA* 3, 631 (R98)

Sutherland, W.J., 1988, *MNRAS*, 234, 159

Sutherland, W.J., Tadros, H., Efstathiou, G., Frenk, C.S., Keeble, O., & Maddox, S., McMahon, R.G., Oliver, S., Rowan-Robinson, M., Saunders, W., & White, S.D.M., 1999, *MNRAS* 308, 289 [astro-ph/9901189]

Szalay, A. S., 1998, in *Proceedings of 18th Texas Symposium on Relativistic Astrophysics*, eds. A. Olinto, J. Frieman, and D. Schramm, World Scientific, Singapore, p. 136

Tadros, H., Efstathiou, G. & Dalton, G. 1998, *MNRAS*, 296, 995 (T98)

Tago, E., Einasto, J., Einasto, M., Hasinger, G., Müller, V., & Andernach, H. 2001, (submitted to *ApJ*, Paper II)

Vogeley, M. 1998, *The Evolving Universe*, ed. D. Hamilton, (Dordrecht: Kluwer), p. 395 [astro-ph/9805160]

TABLE A1

The list of rich superclusters of APM clusters

No	N_{CL}	RA_C	δ_C	D_C $h^{-1} Mpc$	Abell-ACO										No.	(7)	
					(1)	(2)	(3)	(4)	(5)	(6)							
1 _c	4	0.1	-62.0	292	38 _e	47 _e	906 _e	932 _e	942	25 _e	32 _e	944	947	951 _e	72	76	9 (Sculptor region)
2	7	1.1	-40.4	286	2 _e	6 _e	9 _e	20	35	51	57 _e	58 _e	59 _e	72	76	5 (Sculptor region)	
3	14	2.9	-34.0	304	3	10	10	10	942	951 _e							
					935	937 _e											
4 _c	5	4.2	-51.3	315	17 _e	23 _e	26 _e	45	45	81 _e							
5 _c	4	5.8	-51.8	250	31 _e	60 _e	70 _e	79	79								
6	24	10.0	-26.7	306	48 _e	55 _e	65 _e	67 _e	73	80 _e	82 _e	87 _e	92	96			9 (Sculptor)
					99	100	101	103 _e	103 _e	104	110	112	119	121 _e	124		
					127 _e	128 _e	130	137 _e									
7 _c	5	12.6	-50.2	319	102 _e	111 _e	113 _e	129 _e	135 _e								
8	16	19.3	-35.5	312	123	131 _e	134 _e	144	151 _e	153 _e	164 _e	167 _e	169 _e	174 _e			22
					175 _e	178 _e	180 _e	186 _e	188 _e	199 _e							23
9	4	19.5	-37.0	221	158 _e	160	162	173									
10 _c	4	19.7	-24.8	304	156 _e	159 _e	168 _e	170 _e									
11	4	23.5	-32.8	192	182	193	194	209									
12	4	25.6	-55.0	257	204	211	213	214									
13 _c	8	28.0	-33.8	313	205 _e	206 _e	212 _e	222 _e	230 _e	232 _e	233 _e	235 _e					
14	7	30.4	-41.5	323	215 _e	229 _e	234	236	237 _e	240 _e	242 _e						37
15 _c	4	32.5	-40.4	285	228 _e	246	251 _e	259 _e									37
16	9	34.2	-47.8	310	243 _e	249	250 _e	256 _e	258 _e	262 _e	263	264 _e	267 _e				41
17 _c	4	39.1	-33.5	307	276 _e	277 _e	280 _e	295 _e									43
18	4	41.3	-46.1	275	289	291 _e	297 _e	300 _e									
19	7	41.8	-24.9	309	303 _e	300 _e	291 _e	287 _e	305	309	320						
20 _c	6	43.1	-41.1	318	332 _e	325 _e	321 _e	316 _e	299 _e	293							
21 _c	5	43.6	-51.3	323	301 _e	324 _e	326 _e	327	328								
22	30	46.9	-53.7	201	285	287 _e	296 _e	298 _e	302 _e	304	308 _e	310 _e	314 _e	323 _e	48 (Horologium-Reticulum)		
					330 _e	340 _e	343 _e	346 _e	356	364	380	382 _e	383 _e	389 _e			
					391	395	396	397	399	403	421	434	445	463 _e			
23 _c	7	49.5	-44.5	318	350 _e	351	384 _e	385 _e	390 _e	392 _e	393 _e						48
24	9	50.4	-43.0	179	342	358 _e	360	365	387	388	413	415	443				48
25	16	51.1	-44.3	209	357	362	366	367	369	370	372 _e	373	374	377			
26	23	52.3	-32.5	294	375 _e	376 _e	378 _e	379 _e	381 _e	394 _e	401 _e	402 _e	406 _e	407	53 (Fornax-Eridanus)		
					409 _e	412 _e	414	416	418	419 _e	422 _e	423	424	426 _e			
27 _c	15	61.1	-29.9	305	457 _e	458 _e	460 _e	461 _e	466 _e	467	471 _e	472 _e	482 _e	487 _e			
28 _c	5	69.4	-26.0	278	498	507 _e	526 _e	535 _e	537 _e								65
29 _c	11	69.6	-46.2	317	501 _e	512 _e	514 _e	521 _e	522 _e	523 _e	528 _e	529 _e	534 _e	543 _e			
30 _c	4	74.3	-29.6	283	539 _e	561 _e	563 _e	564 _e									
31 _c	7	76.7	-43.2	305	546 _e	565 _e	570 _e	576 _e	580 _e	594 _e	598 _e						
32 _c	4	77.5	-29.2	316	568 _e	569 _e	581 _e	599 _e									
33	7	77.9	-41.4	225	575 _e	577 _e	578	583	585	593	601						
34 _c	4	78.2	-42.4	272	584 _e	588 _e	596 _e	597 _e									
35 _c	4	311.2	-32.4	313	606 _e	608	610 _e	612 _e									
36 _c	4	315.8	-35.5	324	618	622 _e	628 _e	632 _e									
37 _c	11	318.0	-42.7	313	619 _e	624 _e	627 _e	630	633 _e	639 _e	640 _e	649 _e	652 _e	655 _e			
					667 _e												
38	8	318.8	-45.8	275	634 _e	635 _e	641 _e	642	650	653	657	659					183
39 _c	7	319.1	-43.9	214	625 _e	637 _e	644	645 _e	647 _e	658 _e	681 _e						
40 _c	4	325.4	-51.5	315	689	691 _e	698 _e	705 _e									182
41	4	325.8	-42.2	180	688	700	709	711									190
42	5	326.8	-32.1	257	674	693 _e	714 _e	721	749								
43	8	328.6	-19.1	305	704 _e	718 _e	723 _e	728 _e	735	737 _e	741	745 _e					
44 _c	4	328.7	-57.3	308	712 _e	719 _e	730 _e	736 _e									
45	4	331.4	-69.6	192	731	739 _e	740	756 _e									
46	14	332.8	-56.7	216	685 _e	695 _e	708	717 _e	726	732	744 _e	766	776	777			192
					780	788 _e	790 _e	792									
47	10	336.4	-48.8	295	754	769 _e	770 _e	773 _e	778	781 _e	782	787	793 _e	796 _e	197 (Grus)		
48 _c	6	338.7	-37.9	312	794 _e	795 _e	797 _e	798 _e	799 _e	803 _e							
49	4	341.1	-45.2	255	811	812	814	815									197 (Grus)
50	5	342.3	-64.6	272	774	813	822	837 _e	849 _e								200
51	10	345.2	-30.8	304	827	831 _e	832 _e	836 _e	840	847 _e	853 _e	864	868 _e	869 _e	209		
					896 _e	903 _e											
52	4	348.9	-42.1	309	861 _e	878	883	885 _e									209
53	12	349.8	-22.9	311	862	866	876 _e	880 _e	881 _e	887 _e	888 _e	889 _e	890	894 _e			
					897 _e	899 _e	912 _e	913 _e									
54 _c	4	352.6	-32.5	294	897 _e	899 _e	912 _e	913 _e									220 (10 - Pisces-Cetus)
55	7	358.9	-34.2	147	1	5	12	905	933	938	945						